Structural Engineering and Mechanics, Vol. 3, No. 5 (1995) 475-495
DOI: http://dx.doi.org/10.12989/sem.1995.3.5.475

Application of the compressive-force path concept in the design of reinforced concrete indeterminate structures: A pilot study

Salek M. Seraj†

Bangladesh University of Engineering and Technology, Dhaka, Bangladesh

Michael D. Kotsovos‡

National Technical University of Athens, Greece

Milija N. Pavlović‡†

Imperial College of Science, Technology & Medicine, University of London, UK

Abstract. In the past, physical models have been proposed, in compliance with the concept of the compressive-force path, for the realistic design of various statically determinate structural concrete members. The present work extends these models so as to encompass indeterminate RC structural forms. Pilot tests conducted on continuous beams and fixed-ended portal frames have revealed that designing such members to present-day concepts may lead to brittle types of failure. On the other hand, similar members designed on the basis of the proposed physical models attained very ductile failures. It appears that, unlike current design approaches, the compressive-force path concept is capable of identifying those areas where failure is most likely to be triggered, and ensures better load redistribution, thus improving ductility. The beneficial effect of proper detailing at the point of contraflexure in an indeterminate RC member is to be noted.

Key words: compressive-force path; continuous beam; indeterminate structures; physical model; portal frame; reinforced concrete; structural design; tests.

1. Introduction

The present paper describes a first attempt to extend the applicability of the compressive-force path (CFP) concept (Kotsovos 1988) (which, so far, has been successfully applied to the design of simply-supported reinforced- or prestressed-concrete beams (Kotsovos and Lefas 1990, Seraj, Kotsovos and Pavlović 1992a, 1992b, 1993a, 1993b, 1995) and shear walls (Lefas, Kotsovos and Ambraseys 1990)) to the design of indeterminate skeletal structures. First, the possible application

† Assistant Professor
‡ Professor
‡† Reader

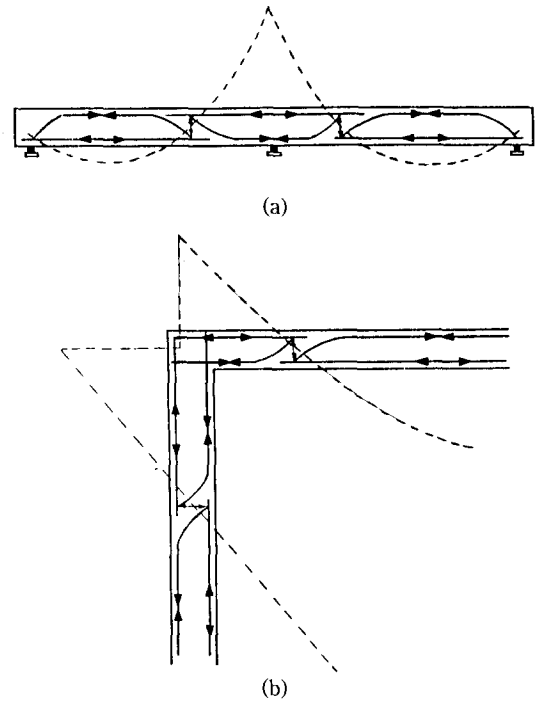

Fig. 1 Proposed model for (a) continuous beam, and (b) frame.

of the "tied-frame" model (Kotsovos and Lefas 1990) to continuous beams and portal frames is explored. Then, the results of pilot tests performed on continuous beams and portal frames are reported, thus showing how the simple physical model developed originally for simply supported girders, can be applied to more complex (indeterminate) structural forms.

2. Physical models for indeterminate RC members

The CFP method of design can be extended to any skeletal structural-concrete configuration, with the "tied-frame" model being used to represent elements between consecutive points of inflection and the regions including such points being modelled as "internal supports" to allow for the interaction of the two adjacent portions of the structure. At the internal supports, the reaction is equal to the shear force that develops in the section through the point of inflection. The provision of web reinforcement in the form of stirrups by an amount sufficient to sustain the action of the shear force should yield a satisfactory design solution. It has been proposed that such reinforcement should extend over a length equal to "2d" symmetrical about the point of inflection to allow for possible shifting of the latter if plastic hinges are formed sequentially prior to collapse. Considering the fact that concrete is very weak in tension, it is suggested that only a minor contribution (say, of the order of 0.5 MPa) from concrete can be considered in designing such internal supports. This design approach has been adopted in the present paper for the modelling of a two-span continuous RC beam and a fixed-ended portal frame. Initially, these indeterminate structures have been transformed into a number of determinate structural elements. Fig. 1 shows how the proposed model can be applied to the modelling

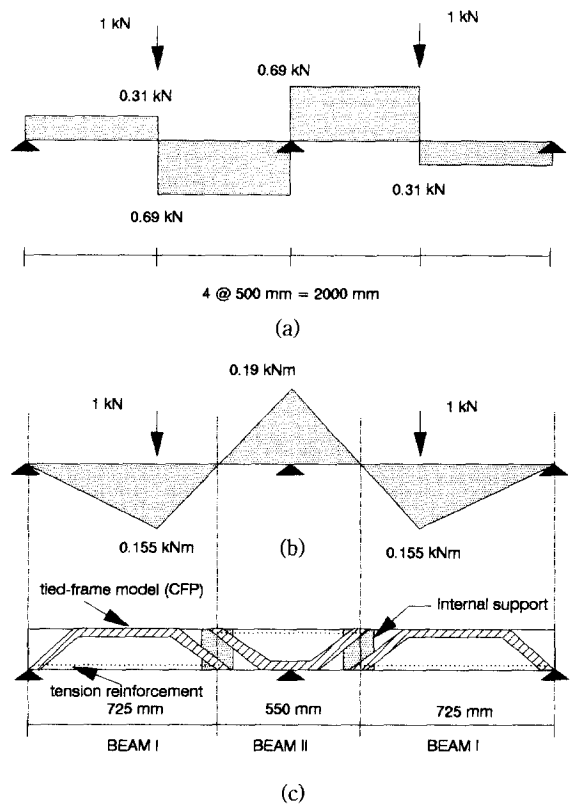

Fig. 2 (a) Shear force, and (b) bending moment diagrams for the continuous beams tested, when subjected to unit loads at the middle of each span, and (c) schematic representation of RCCB4 according to the proposed model.

of such RC continuous beams and portal frames. It is important to mention here that the design of individual "statically determinate" structural elements, separated by the internal supports, follows the design method described elsewhere (Kotsovos and Lefas 1990, Seraj 1991).

3. Experimental study of RC continuous beams

3.1. Beam and testing details

Two RC continuous beams have been tested and will be reported in this paper. The beams had two equal spans of 1000 mm each with an overhang of 75 mm beyond the supports. They were loaded equally at the middle of each span. In Figs. 2a and 2b, the relevant shear force and bending moment diagrams, considering elastic behaviour due to unit loads at the loading points, have been shown. From these diagrams, the actual ultimate shear force and bending moments acting at different sections of the beams to be studied can be calculated, by multiplying all the ordinates of the shear force and the bending moment diagrams with the ratio of the flexural moment capacity of the member to the maximum bending moment at the innermost support (0.19 kNm). (This is a slightly approximate method but is in keeping with the BS 8110 (1985) guidelines which suggest the use of elastic-behaviour diagrams, and then to allow for

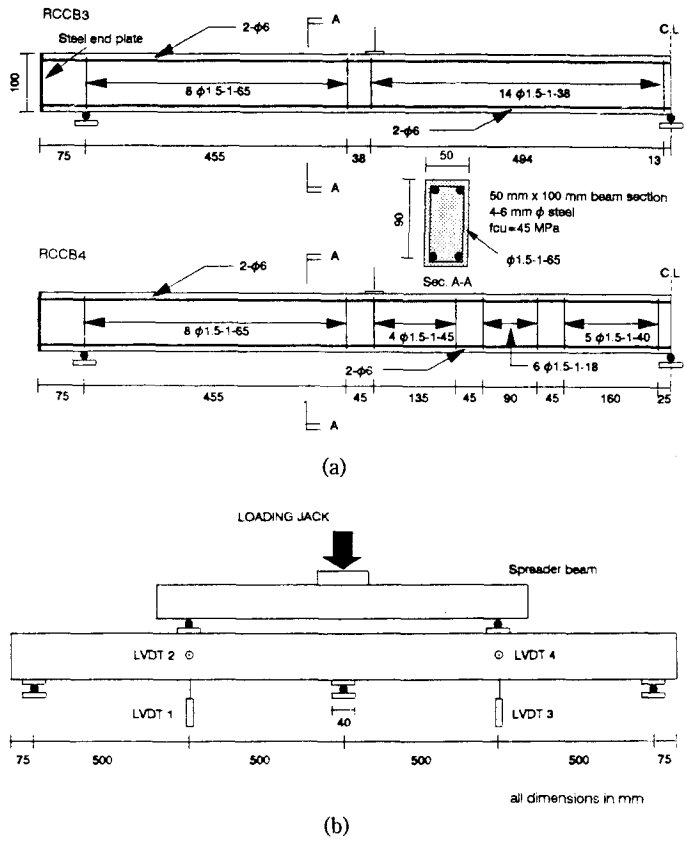

Fig. 3 (a) Dimensional, cross-sectional and design details, and (b) schematic representation of the rig of the RC continuous beams tested.

redistribution. Although a more rational approach would have been to use plastic-behaviour diagrams, in the design of the beam it was originally questioned whether all its hinges would, in fact, be attained in the experiment (as it turned out, full plasticity seems to have been achieved - see later). Clearly, "elastic-" and "plastic-" behaviour diagrams should bound peak values and location of inflection points.) The "discretization" of the continuous beam designed in accordance to the CFP concept (denoted as RCCB4) has been portrayed in Fig. 2c.

The dimensional, cross-sectional and general design details of the RC continuous beams RCCB 3 and RCCB4, designed to the British Code and the proposed method respectively, are presented in Fig. 3a; whereas Fig. 3b is a schematic representation of the experimental rig. The width of the internal support, in RCCB4, has been considered to be equal to the effective depth "d", in contrast to the originally proposed width of "2d". This was necessary in an attempt to eliminate possible overlapping of the zone of the internal support with the zone where the CFP changes its direction in the individually-modelled discretized determinate beams (into which the continuous beam has been divided). Thus, it was thought that, for the type of continuous RC beams investigated, the role of separate modelling of the internal support could be more clearly identified, in these initial pilot tests, by localizing the width of influence of such zones, rather than spreading it over a wider area.

The beams were cast using a 45 MPa cube strength concrete mix (51.2 MPa on test day) (Seraj 1991). The yield stress of 6 mm and 1.5 mm diameter steel used were 570 MPa and

Table 1 Predicted and measured load-carrying capacity, and recorded failure type, of the RC continuous beams tested

Beam	Total sustained load, kN				Failure type
	Predicted			Measured	
	BS 8110	ACI 318	CFP		
RCCB3	30.11	24.15	30.11	41.72+0.84*=42.56	Brittle
RCCB4	28.31	23.59	30.11	42.01+0.84*=42.85	Ductile

*weight of spreader beam

460 MPa, respectively. The ultimate strengths of these bars were 665 MPa and 510 MPa. The design calculations of RCCB4 have been described in Appendix A. Details of the testing procedure. loading sequence, and validation of the testing set-ups are available elsewhere (Seraj 1991).

4. Discussion of RC continuous beam results

4.1. Load-carrying capacity

The load-carrying capacity of beams RCCB3 and RCCB4, as calculated by using BS 8110 (1985), ACI 318 (1989) and the proposed method are given in Table 1. It is interesting to note that the failure loads predicted by all these methods lie between 55% and 70% of the actual failure load. An explanation of the discrepancy between the actual and calculated failure loads is given in Appendix B.

4.2. Deformational response

The load-deflection relationships of RCCB3 and RCCB4 are shown in Fig. 4a. The figure shows that, while beam RCCB3 underwent a brittle type of failure, the deformational response of RCCB4 was very much ductile. At failure, the midspan deflection of RCCB4 was, in fact, twice the magnitude of the deflection of RCCB3.

4.3. Cracking process

The cracking process, in both the beams, started with the formation of nearly vertical cracks which developed simultaneously below the loading points and above the central support. With increasing load, these cracks grew in length and, also, new inclined cracks, oriented towards the loading points and the central support, were formed. Failure occurred along the outermost crack from the point load in the case of RCCB4, and along the outermost crack from the central support for RCCB3. The extent of cracking and the orientation of the failure crack are shown in Fig. 4b, the centre of the uncracked zones being in close agreement with the position of the point of inflection. The cracking of RCCB3 was more centralized around the vicinity of the central support and the cracks along which failure occurred had developed steadily as the load increased. On the other hand, in RCCB4, cracking was evenly distributed over all the three critical points, and the extent of cracking was very much enhanced near failure indicating its greater potential for stress redistribution and superior ductility. Just before failure, flexural cracks having widths of the order of 1-1.5 mm were visible over the central support and below the loading points. At an applied load of 42 kN, when the critical flexural crack was almost

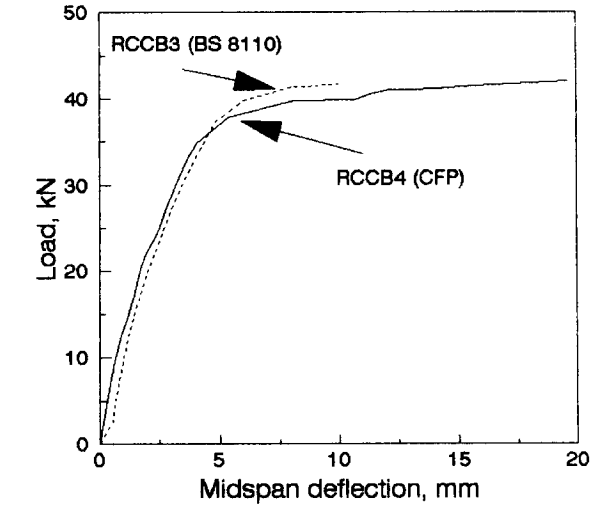

(a)

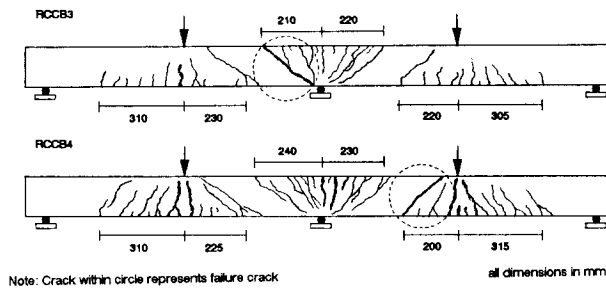

(b)

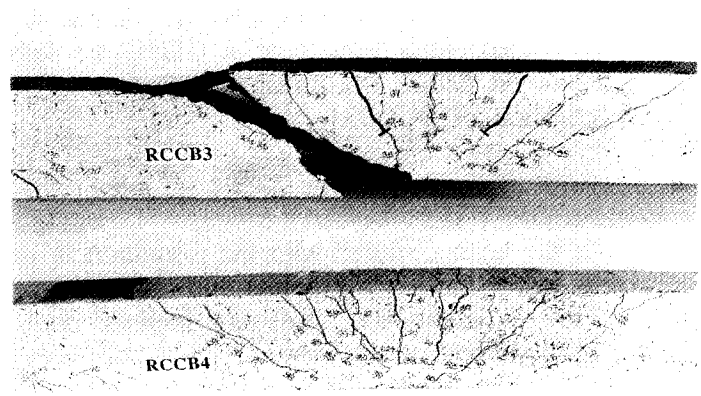

(c)

Fig. 4 Performance of the RC continuous beams tested: (a) Load-midspan deflection curves; (b) extent of cracking and orientation of failure crack; (c) crack pattern at central support zone after failure.

imminent, a diagonal crack penetrated into the compressive zone and failure took place. At this stage, the transverse reinforcement snapped. Fig. 4c shows the crack patterns, after failure, at the central support zone of the beams tested. The ductility of RCCB4 is clearly noticeable from this figure.

4.4 Causes of observed behaviour and failure mechanism

For both the beams tested, the amount of transverse reinforcement furnished was actually designed for sustaining stresses which turned out to be about 30% less than the stresses which were actually borne at the critical sections at failure. Clearly the shear reinforcement in the beams tested was inadequate. However, this cannot be the cause of failure. It has been mentioned in the previous section that the beam RCCB4, designed to the proposed (CFP) method, was substantially more ductile than its British Code counterpart, RCCB3. In reality it contained even less reinforcement in most part of the shear span in comparison to RCCB3. The beam RCCB4, however, had additional transverse reinforcement at the internal support within the shear-critical span. The crack causing ultimate failure of RCCB3 was situated near the central support, a zone containing more shear reinforcement than RCCB4. On the other hand, for RCCB4, the location of such cracking was nearer to the loading points. It appears that the transverse reinforcement provided in RCCB4 (in order to make an effective internal support at the point of inflection, as advocated by the proposed method) played an important role in bringing RCCB4 to a very ductile failure. It has been the additional transverse reinforcement in the region of the internal support that prevented shear failure and led to ductile collapse of RCCB4. It helped in the smooth "flow" of load throughout the whole structure by distributing moments from the more stressed to the less stressed regions. It is important to note that the favourable consequences due to the presence of such reinforcement cannot be explained by the traditional truss-analogy concept (Ritter 1899, Mörsch 1902), as this reinforcement was confined to a narrow width of only 90 mm (equivalent to only 18% of the shear span). It also appears that underestimation of the flexural capacity when designing in compliance with current practice may result in lack of safety (thus, the use of elastic internal-action diagrams leads to smaller shear forces than those attained when (plastic) redistribution is to be allowed for).

5. Experimental study of RC portal frames

5.1. Frame details

Two portal frames have been investigated and are reported in this paper. The frames designated as PF1 and PF2 were designed to the British Code BS 8110 (1985) and the proposed (CFP) method respectively. Fig. 5 contains the dimensional, cross-sectional and the other design details of these frames. The footings attached to the columns of the frames were post-tensioned to the testing floor of the laboratory so as to ensure total fixity at the base of the columns.

The portal frames were tested so that they would be initially subjected to a vertical loading at the midspan of the beam. Then, keeping the vertical load constant, the frame would be loaded to failure by applying a horizontal load acting at the centroid of the beam section. In Figs. 6a and 6b, the elastic shear force and bending moment diagrams, due to design forces of 24 kN (vertical) and 20 kN (horizontal) applied to a frame having centre-line dimensions equal to the frames under study, are shown. The "discretization" of the portal frame PF2 according to the CFP concept has been delineated in Fig. 6c. On the other hand, PF1 has been designed using the British Code provisions.

For the relevant design calculations of PF1 and PF2, Seraj (1991) should be consulted, as well as Appendix A. The main reinforcement of the frame consisted of 6-10 mm ϕ high-yield steel. The moment capacity of the beam and of the column sections was such that nominal

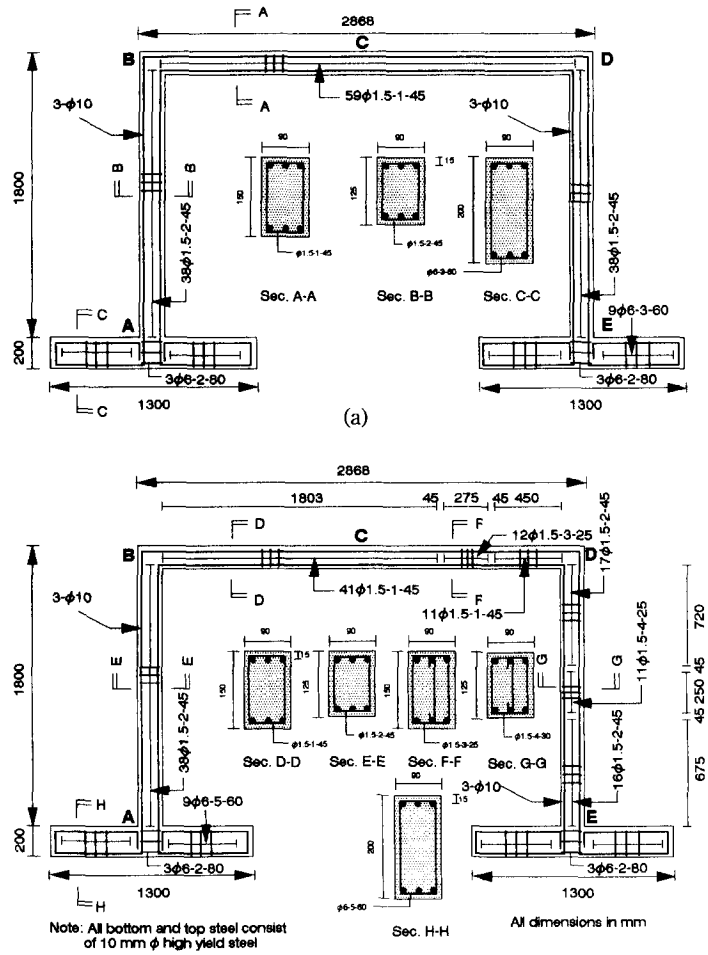

Fig. 5 Dimensional, cross-sectional and design details of RC fixed-ended portal frames (a) PF1, and (b) PF2.

shear reinforcement, in accordance to the British Code provisions, was sufficient to cater not only for the design shear forces, but also for a certain excess of these. For example, for the above-mentioned type of loading, the beam of the frame is subjected to a maximum shear force of 17.45 kN (shown in Fig. 6a). However, the beam section, furnished with nominal reinforcement, can sustain shear forces up to 23.22 kN. A nominal amount of transverse reinforcement was also found to be adequate for the frame PF2 at locations where the CFP changes its direction in all the discretized determinate beams that make up the portal frame designed to the proposed method. The furnished transverse reinforcement for both frames was found to be compliant with the ACI Code provisions, as well.

It is necessary to point out, at this stage, that the purpose of testing the frames PF1 and PF2 was to visualize the importance of designing structural members based on realistic physical models. It has been found earlier that modelling the point of inflection, in an indeterminate member, as an internal support results in a ductile, and thus safer, design solution. It was in keeping with the approach adopted in the design of the continuous beams that the testing program of the portal frames was conceived. Only nominal transverse reinforcement was provided at

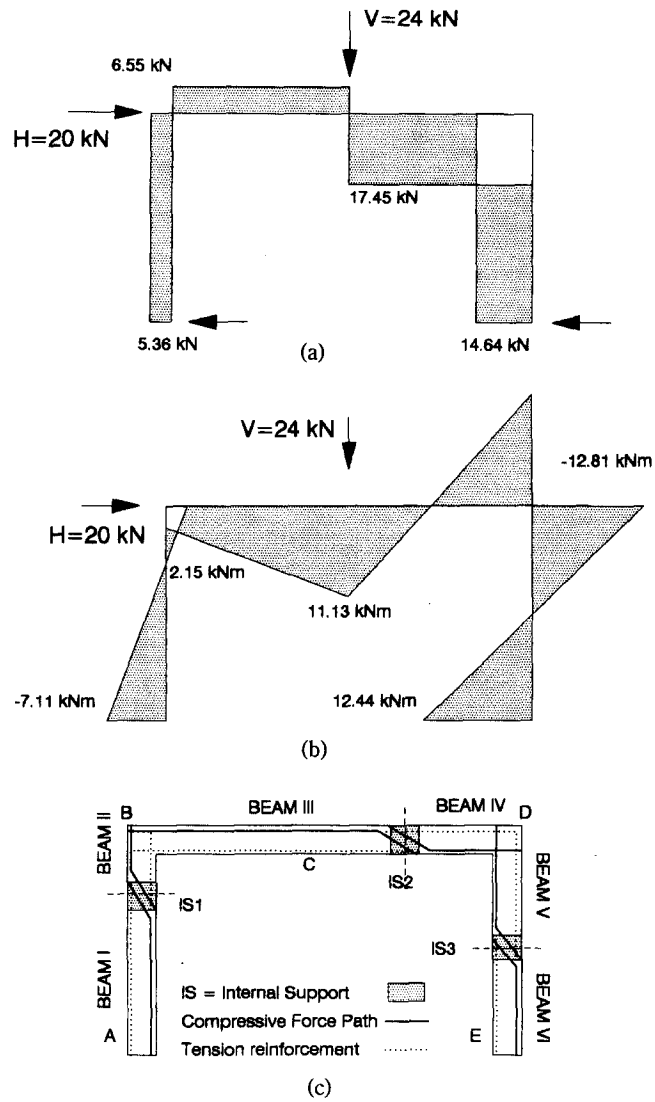

Fig. 6 (a) shear force, and (b) bending moment diagrams of the fixed-ended portal frames tested, when subjected to vertical and lateral loading, and (c) schematic representation of PF2 according to the proposed model.

all locations for frame PF1 (since, according to BS 8110 no design shear reinforcement is required), and the same applied to frame PF2 except that the latter was given the necessary shear reinforcement at the critical points of inflection ("internal supports") IS2 and IS3 (the IS1 reinforcement was already covered by the nominal reinforcement); the latter locations are shown in Fig. 6c. It is obvious that the effect of modelling internal supports can best be observed by comparing the test results of the portal frames under consideration, because in all other respects the two frames are similar. Since the precise nature and direction of the loading of the frame was known, the additional reinforcement required by the internal supports IS2 and IS3, in PF2, was provided only in the right column and in the right half of the beam. The width of such supports has been considered to be equal to the originally proposed width of "2d", thus catering for the

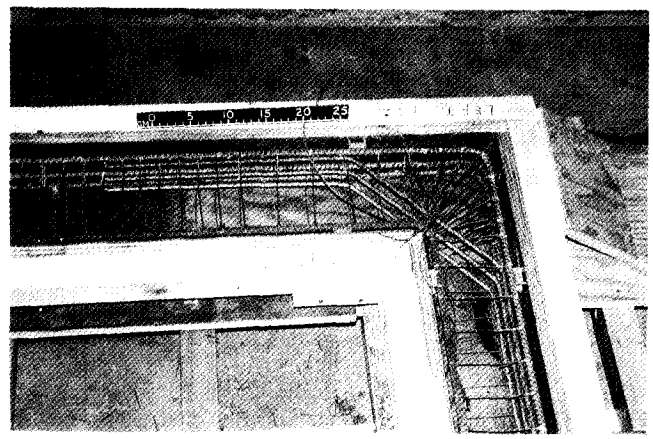

Fig. 7 Corner reinforcement in the portal frames.

possible variation in the location of points of inflection, at the ultimate limit state, due to a probable shift of the moment diagram in the course of transition from the elastic to the plastic stage. In actual practice, of course, the reinforcement on both sides of a frame should be provided symmetrically, in order to cater for wind or earthquake forces coming from either direction.

It is worth mentioning here that both the frames were provided with the necessary amount of corner reinforcement at the beam-column intersection following standard design practice. The detailed arrangements of the corner reinforcement, placed within the mould, at the opening corner (corner at B) may be seen in Fig. 7. The portal frames were also cast from a 45 MPa cube strength concrete mix (around 48 MPa on test day). The yield and ultimate strengths of 10 mm diameter main steel used in the frames were 560 MPa and 680 MPa, respectively.

5.2. Testing

The experimental rig and instrumentation of the portal frames studied are shown in Figs. 8a and 8b, respectively. The loading system was designed intending to apply incremental vertical loading at the middle section of the frame and then, without applying any further vertical load to the beam, fail the specimen by employing increasing lateral (horizontal) load at the top of the frame. A tension jack, when energized, pulled down an auxiliary steel framework, and thereby applied vertical loading to the frame. On the other hand, a compression jack subjected the frame to horizontal loading by acting laterally against the beam-column intersection of the frame.

6. Discussion of RC portal-frame results

6.1. Load-carrying capacity

The vertical and horizontal loads recorded by the data logger, at the time of failure, were similar for both portal frames. At the end of the vertical loading, PF1 was subjected to a vertical load of 23.72 kN at the middle of its beam member (see point C in Fig. 8b). The corresponding load for PF2 was recorded as 23.69 kN. Maintaining these vertical loads in the loading machines, the frames were then loaded laterally at the top left corner of the frame (see point B in Fig. 8b). Failure took place when PF1 and PF2 were subjected to a lateral force of 20.0 kN and

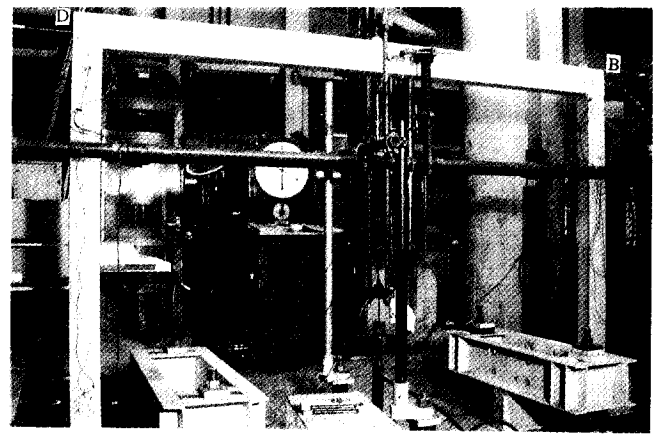

(a)

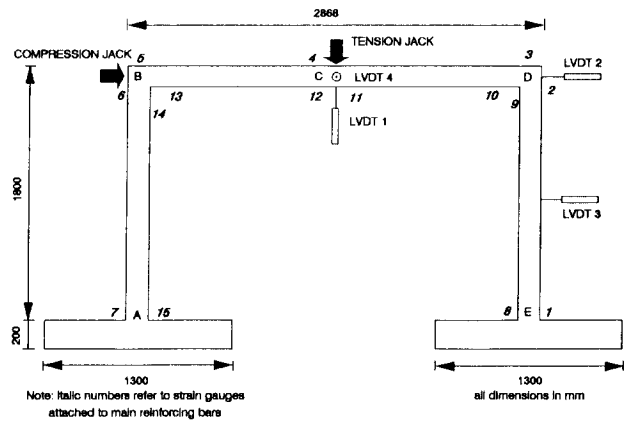

(b)

Fig. 8 (a) Rig, and (b) instrumentation used for testing RC fixed-ended portal frames.

Table 2 Estimate of the actual V load from strain-gauge readings (see Fig. 8b for strain-gauge locations 4 and 11)

Frame	At the end of load V			At the end of load $V+H$					
	$\varepsilon_{11}\times10^6$	$\varepsilon_4\times10^6$	M_c, kNm	$\varepsilon_{11}\times10^6$	$\varepsilon_4\times10^6$	M_c, kNm	Applied V, kN	Calculated V, kN	Applied H, kN
PF1	1679	−514	9.76	2033	−744	11.73	23.72	28.50	20.00
PF2	1596	−584	9.32	2313	−892	13.26	23.69	33.68	19.95

19.95 kN, respectively. The deformational responses of these frames, however, were quite different. While such responses will be discussed in detail later, it is important to show, at this stage, that, due to the difference in their deformational behaviour, the two frames were in fact subjected to different loadings at failure. For fixed-ended portal frames like PF1 and PF2, the moment at point C (Fig. 8b) is due to the vertical loading at that point alone, as the adopted horizontal loading does not produce any moment there. Table 2 contains the micro-strain readings of the bottom- and top-steel at point C. From these readings, using the simplified stress block of BS 8110 (see Fig. A1 of Appendix A), the moment developed at the beam section at C has

been approximately calculated and given in Table 2. (In these calculations, the effect of the axial force has been ignored.) Clearly, due to the different methods of modelling adopted in the design of the portal frames PF1 and PF2, the distributions of moment in these frames are dissimilar, as evidenced by the different amounts of sway. Now, the moment at C due to the vertical loading in the frames can be approximately (on assumptions of linearity) considered to be proportional to the loading throughout the whole loading history. As such, the additional vertical force (at any time) due to the pulling-down effect of the rig due to sway (see Appendix C for details) may be estimated by knowing the moment at point C and the vertical loading applied on the frame prior to the introduction of the horizontal loading. Adopting this method and using the moment values calculated from the strain readings at failure, the actual vertical load at C has been calculated and summarized in Table 2. It appears that the frame PF2 failed at a vertical load approximately 18% higher than that for frame PF1. Moreover, it should be noted that, in both frames, the actual V was substantially higher than the V applied by the tension jack (~23.7 kN); this was due to the pulling-down effect caused by sway (see Appendix C).

6.2. Deformational response

The vertical displacement at C (δ_C) and the horizontal displacement at D (δ_D) due to vertical and horizontal loadings have been plotted in Figs. 9a and 9b, respectively. In this figure, the legends "PF2, V" and "PF2, H" refer to the displacement observed in the portal frame PF2 due to vertical loading, and combined vertical and horizontal loading, respectively. (Note that ordinates refer to individual loads.) Similar legends have also been used for PF1. From the figures, it is clear that the frame PF2 was more ductile than the frame PF1. The variation of bottom-steel strain (ε_{11}) and top-steel strain (ε_4) at C are plotted, against the applied loading, in Figs. 9c and 9d, respectively. The additional strain readings in the steel elements of PF2 at failure, both in the compression and in the tension side, emphasizes the point that the middle section of the beam corresponding to PF2 was subjected to higher flexural stresses than that of PF1, as a result of the large sway effect. It is also evident that, during the initial stages of the application of horizontal load, there has been very little increase in ε_{11} and ε_4. This finding is in line with the observation made in Appendix C, where it has been found that the present loading is affected by side sway only when large amounts of lateral displacements take place. The variation of top-steel strain reading at corner D (ε_3) has been plotted against applied load in Fig. 9e. It appears that the steel at this location was much more strained in PF1 than in PF2, indicating that the corner D in PF1 was subjected to more rotation in comparison to PF2. A plausible explanation for the above finding can be derived from Fig. 9f, where the variation of steel strain readings ε_8 at the inner side of E (foot of the right-hand side column) has been plotted against the applied load. Although the steel elements in both frames had reached the yield stress, it is the steel in PF2 that was exposed to plastic deformation. It appears that rotations at points D and E, due to moments, were shared and/or transferred more uniformly in the case of PF2 than in PF1, for the latter one it being more concentrated at corner D. An inspection of the steel strain readings ε_7 and ε_{15} at A indicated that a plastic hinge was also formed at the foot of the left-hand side column in PF2 at failure. In the case of PF1, the bending moment at A at collapse was also approaching the member's flexural capacity.

6.3. Cracking process

The cracking process of the portal frames tested can be described by reference to Fig. 10,

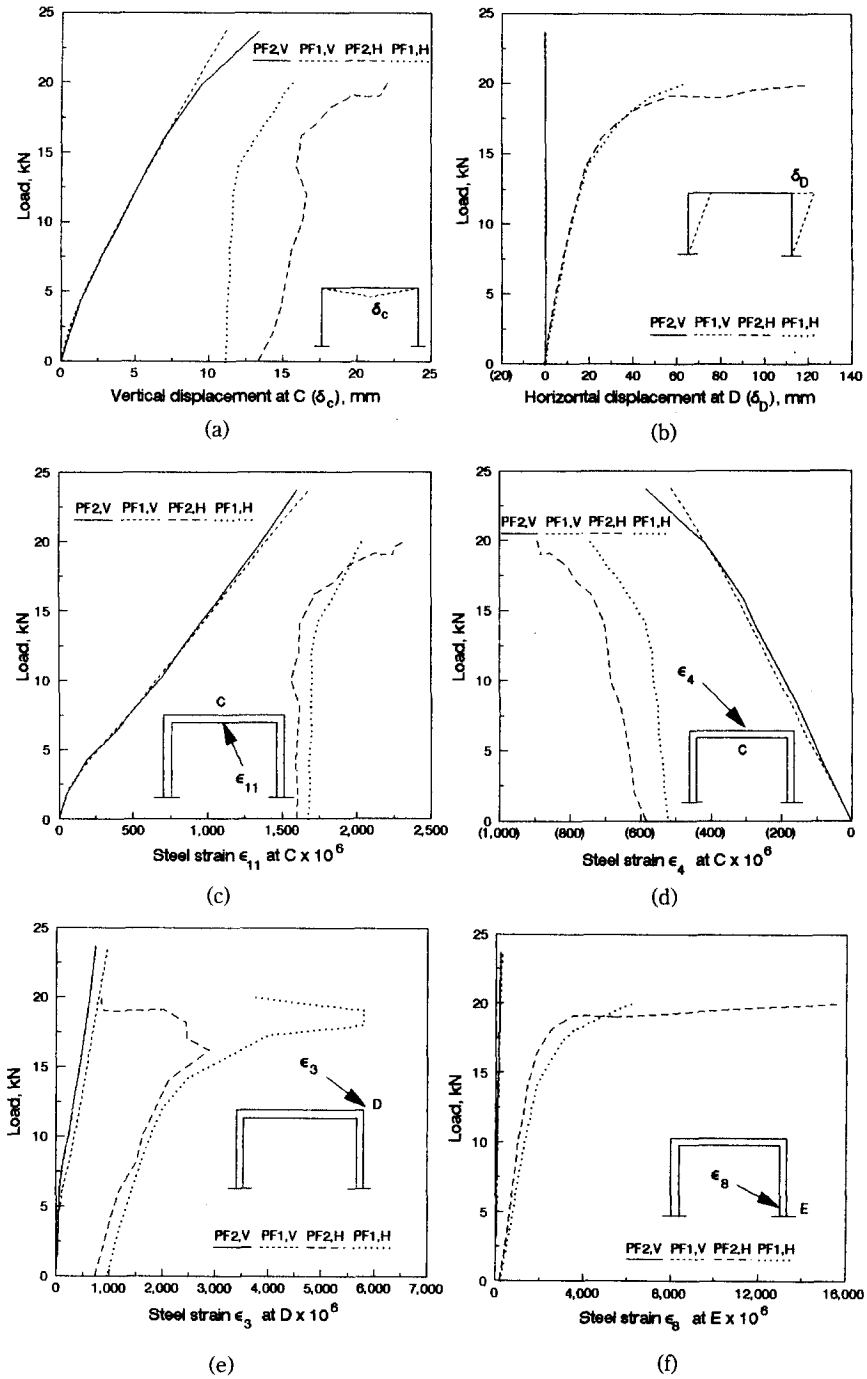

Fig. 9 Load versus (a) vertical displacement δ_c, (b) horizontal displacement δ_D, (c) steel strain ε_{11}, (d) steel strain ε_4, (e) steel strain ε_3, and (f) steel strain ε_8 due to vertical loading (V), and combined vertical and horizontal loading (H). (Note that ordinates refer to individual loads.)

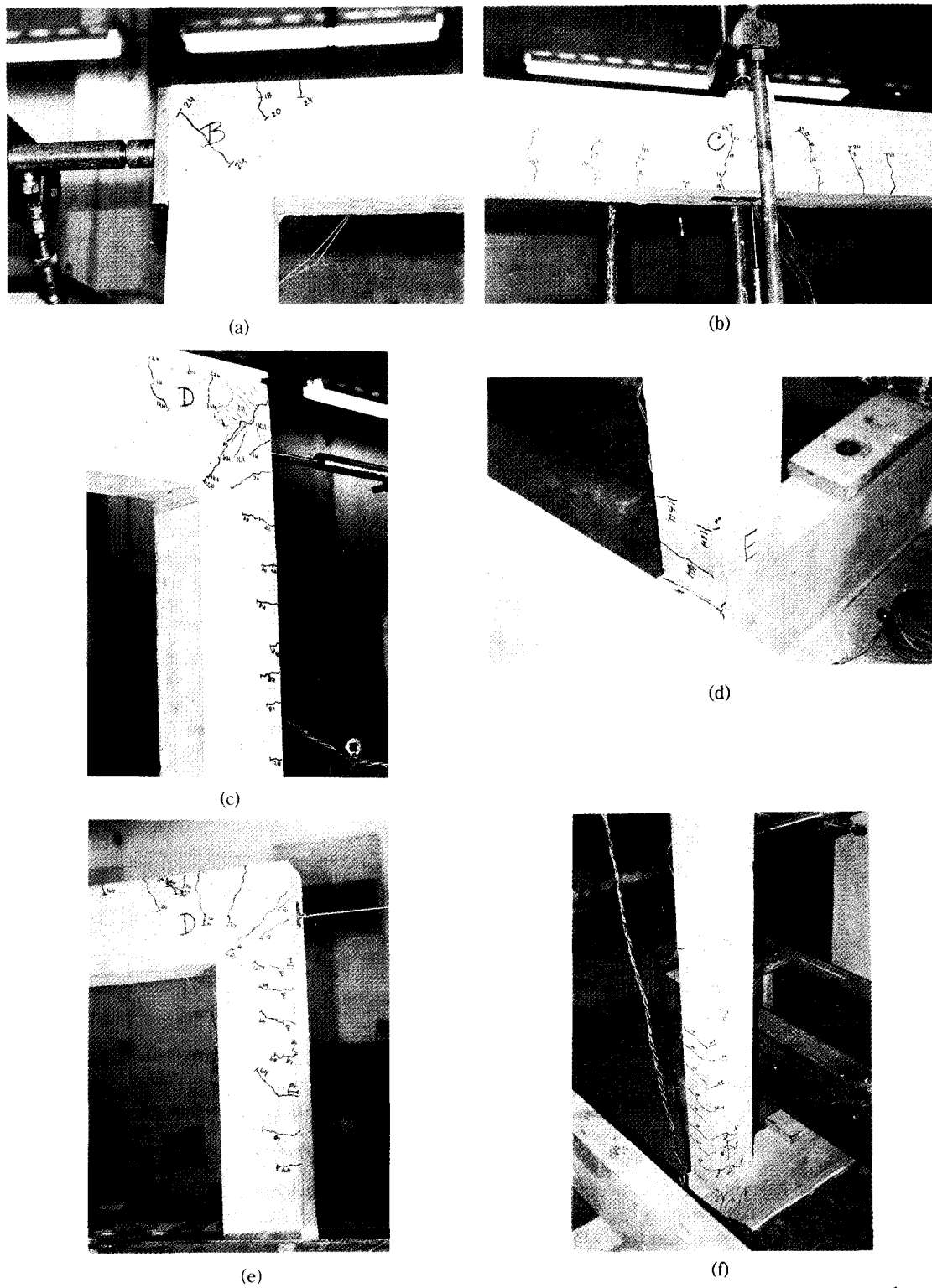

(a) (b) (c) (d) (e) (f)

Fig. 10 Cracking pattern just before failure at (a) B, (b) C, (c) D, and (d) E for PF1, and at (e) D and (f) E for PF2.

which shows the crack patterns just before failure for PF1 (at B, C, D and E) and PF2 (at D and E). (The crack patterns of PF2 at B and C being very much akin to those for PF1, are not included.) The first flexural crack took place near the midspan, in both the frames, at a vertical load of 10 kN. With the increase of vertical load, more cracks appeared in the middle part of the beam and gradually propagated upwards. The flexural crack at the centre of the beam was found to be the deepest fissure at the end of the vertical loading. Cracks also appeared at the top of the beam-column intersection at B and D, when the vertical load approached 18 kN. Diagonal cracks at both corners were visible at an applied vertical load of about 24 kN. Once again, these observations are applicable to both frames.

While the crack patterns of PF1 and PF2 were similar throughout the application of the vertical loading, significant variations were detected during the application of the lateral loading. Flexural cracks appeared at the corner D of both frames at an applied horizontal load of 2 kN. With an increase in the amount of horizontal load, more cracks gradually appeared in the top right half of the column DE; however, the depth of these cracks was less in the case of PF1 than for PF2. On the other hand, for PF1, the cracks were more intense near the corner D, while only a few cracks could be detected in the tension side of the base of the column DE. By contrast, in the case of PF2, cracks were almost evenly poised on the tension side of both halves of the column DE. At loads near failure, a few cracks were visible at the bottom of column AB of PF2; no such cracks were detected in PF1. Ultimately, failure in PF1 took place due to excessive cracking at the corner D, where wide diagonal cracks and spalling of concrete was detected at collapse. On the contrary, frame PF2 failed almost like a mechanism when the diagonal cracks at corner D became wide and the steel at the tension side of the column footings gave in.

6.4. Causes of observed behaviour and failure mechanism

It has already been estimated that the failure of PF2, designed to the proposed (CFP) method, took place at an applied vertical load which was about 18% greater than the corresponding load sustained by its British Code counterpart, PF1. Both frames were subjected to almost equal amounts of load laterally. More importantly, while the failure of PF2 was marked by very ductile deformational behaviour, the response of PF1 was quasi-ductile. Thus the displacement ductility of PF1 (taking the ratio of δ_D (see Fig. 9b) at collapse and storey height h) was about 3.3%; the value of δ_D at collapse being 60 mm and h being 1800 mm. On the other hand, for PF2, displacement ductility was 6.7%, considering δ_D of 120 mm, which was well past the limit of structural usefulness. It is interesting to note that in PF1, like the RC continuous beam RCCB3 reported earlier, cracking was more concentrated in the vicinity of the maximum negative moment. It appears that PF1 was incapable of distributing moments from the highly stressed regions to its neighbouring, less stressed, regions. This resulted in a heavy concentration of moment localized around the point D. Consequently, premature failure took place at the beam-column corner at D. On the other hand, although the corner reinforcement in PF2 was exactly the same as that of PF1, both the zones D and E (and, to a lesser extent, A) underwent considerable amounts of deformation before failure took place after allowing the frame to undergo large values of side sway. The nominal moment capacity of the beam section being 16.05 kNm (Seraj 1991), the calculated moment of PF2 at the beam section through C at failure (13.26 kNm) was found to be less than this nominal moment-carrying capacity of the section. However, from the relevant column interaction diagram, it was shown elsewhere (Seraj 1991) that, at an applied moment of 13.7 kNm, failure can just take place in the column. The applied moment at E,

as calculated from the strain readings of PF2, was in fact 13.9 kNm, and hence the formation of plastic hinges at D and E was likely. (Note that the moments at A, C, D and E are all very similar.) The extensive cracking at the footing and the top of column DE of PF2 (see Figs. 10e and 10f) points to such a possibility. It is obvious that the additional links placed at the points of inflection, in PF2, make all the individual structural elements an integral part of the whole skeletal structure, by ensuring proper interaction between them. Thus, moment does not remain restricted, in RC continuous members, to regions subjected to initial deformations provided the structure is realistically modelled and properly detailed. In this respect, the additional transverse reinforcements acting primarily as internal supports help in the formation of plastic hinges in all the prospective locations. This prevents premature failure and adds to the ductility of the structure as a whole.

7. Conclusions

This paper extends previous findings on statically determinate members to indeterminate ones as regards a more rational and economic approach based on the CFP method. Also, in the past, the potentially large discrepancy in load-carrying capacity between the CFP and code methodology was highlighted for members for which the possibility of shear failure was central to the design problem. Implicit in this was the notion that the strength of elements failing in flexure would not significantly be influenced by the design method. The present pilot study shows that, whereas this is indeed likely to be the case as regards the magnitude of the applied load at collapse, the types of failure (ductile/brittle) can vastly differ.

The importance of providing "internal supports" at the points of contraflexure has been demonstrated from the results of the RC continuous beams and fixed-ended portal frames tested. These internal supports greatly increased the ductility of the continuous beam and the portal frame designed to the proposed (CFP) method. Their Code counterparts, which did not cater for such internal supports, either suffered a brittle or a quasi-ductile type of failure.

Provision of transverse reinforcement at the internal supports allowed the interaction of the different portions of the skeletal structures, and eventually led them to a ductile type of failure. The reason for this lies in the fact that, unlike current concepts, the concept of the compressive-force path is capable of (a) identifying the regions where failure is most likely to be triggered, (b) enabling redistribution of loads to other parts of the structure, and (c) assessing accurately both the location and the amount of reinforcement required to safeguard against brittle failure.

Acknowledgements

The authors owe their thanks to Dr. J. Bobrowski of Jan Bobrowski & Partners for his support and encouragement. The first author would like to express his gratitude to the Association of Commonwealth Universities, UK, for awarding him a Commonwealth Scholarship to carry out research of which the present work forms part. Thanks are also due to Bangladesh University of Engineering and Technology for granting him leave of absence during this research programme.

Notations

A_S area of longitudinal tension reinforcement which continues for a distance at least equal to d

beyond section being considered
A_{sv} area of transverse reinforcement
b beam width
b_1 effective width (presently equal to beam width since section is rectangular)
C compressive force in concrete
C' compressive force in steel
d effective depth (mm)
d' depth of compression face to centroid of compression steel
E modulus of elasticity of steel
f_{cu} uniaxial compressive cube strength of concrete
f_{cyl} uniaxial cylinder strength
f_s tensile stress in tension reinforcement
f_s' compressive stress in compression reinforcement
f_u ultimate stress
f_y yield stress; characteristic strength of tension steel (N/mm^2)
f_{yv} yield stress of stirrup material
h storey height; height of frame
M_c moment corresponding to failure load (Nmm)
M_f flexural capacity (Nmm)
s distance of critical cross-section from support (mm) (equal to shear span for point loading and $2d$ for uniformly distributed loading in RC members)
S_v spacing of stirrups
T tensile force in longitudinal steel
V_a applied shear force
V_c tensile force resisted by concrete alone in region where CFP changes direction
x depth of neutral axis
x' depth of neutral axis considering triaxial conditions
z lever-arm distance
δ_C vertical displacement at C
δ_D horizontal displacement at D
Δ_Z increase in lever arm
ε_i strain in gauge number i
ε_s tensile strain in tension reinforcement
ε_s' compressive strain in compression reinforcement
ϕ bar size
ρ_w tension steel ratio (A_s/bd)
σ'_c nominal triaxial compressive stress
σ_c 0.8 f_{cyl}
σ_{conf} confining pressure required for σ_c to increase to σ_c'
σ_t transverse tensile stress

References

ACI 318 (1989), *Building code requirements for reinforced concrete,* American Concrete Institute, Detroit.

BS 8110 (1985), *Structural use of concrete. Part 1-Code of practice for design and construction,* British Standards Institution, London.

Kotsovos, M.D. (1988), "Compressive force path concept : basis for reinforced concrete ultimate limit design", *ACI Structural Journal,* **85**(1), 68-75.

Kotsovos, M.D. and Lefas, I.D. (1990), "Behaviour of reinforced concrete beams designed in compliance with the concept of compressive force path", *ACI Structural Journal,* **87**(2), 127-139.

Lefas, I.D., Kotsovos, M.D. and Ambraseys, N.N. (1990), "Behaviour of reinforced concrete structural walls: strength, deformation characteristics and failure mechanisms", *ACI Structural Journal,* **87**(1),

23-31.
Mörsch, E. (1902), *Concrete steel construction*, English translation by E. P. Goodrich. (McGraw-Hill, New York, 1909) (Translation from 3rd edition of *Der Eisenbetonbau*, 1st edition, 1902).
Ritter, W. (1899), *Die Bauweise Hennebique*, *Schweizerische Bauzeitung*, **33**(7), 59-61.
Seraj, S.M. (1991), Reinforced and prestressed concrete members designed in accordance to the compressive-force path concept and fundamental material properties, *PhD Thesis*, Imperial College, University of London.
Seraj, S. M., Kotsovos, M. D. and Pavlović, M. N. (1992a), "Three-dimensional finite-element modelling of normal- and high-strength reinforced concrete members, with special reference to T-beams", *Computers & Structures*, **44**(4), 699-716.
Seraj, S. M., Kotsovos, M.D. and Pavlović, M.N. (1992b), "Nonlinear finite-element analysis of prestressed concrete members", *Structures & Buildings*, *Proc. Institute of Civil Engineers*, **94**(4), 403-418.
Seraj, S. M., Kotsovos, M.D. and Pavlović, M.N. (1993a), "Compressive-force path and behaviour of prestressed concrete beams", *Materials and Structures, Research and Testing, RILEM*, **26**(156), 74-89.
Seraj, S. M., Kotsovos, M.D. and Pavlović, M.N. (1993b), "Experimental study of the compressive-force path concept in prestressed concrete beams", *Engineering Structures*, **15**(6), 439-451.
Seraj, S. M., Kotsovos, M.D. and Pavlović, M.N. (1995), "Behaviour of high-strength mix reinforced concrete beams," *Archives of Civil Engineering, Proc. Polish Academy of Sciences*, **41**(1), 31-67.

Appendix A

CFP design calculations for RCCB4

(1) Flexural Capacity (see Fig. 3a)

For the RC continuous beams tested, $A_s=A_s'=56.55$ mm^2, $b=50$ mm, $d=90$ mm, $d'=10$ mm, $f_y=618$ MPa, and $f_{cu}=45$ MPa. Using the method described in Fig. A1, we get $x=15.44$ mm, $f_s=618$ MPa, $f_s'=246.63$ MPa and $M_f=2.86$ kNm. The shear forces and the bending moments acting at different sections of the continuous beams can be found by multiplying all the ordinates of Fig. 2 by (2.86/0.19)

(2) Transverse reinforcement

According to the CFP method (see Kotsovos and Lefas 1990, Seraj, Kotsovos and Pavlović 1992a, 1992b, 1993a, 1993b, 1995), the moment corresponding to the failure load (in Nmm) is given by

$$M_C=0.875 \text{ sd } \left(0.342\ b_1+0.3\frac{M_f}{d^2}\sqrt{\frac{z}{s}}\right)\sqrt[4]{\frac{16.66}{\rho_w f_v}} \tag{A1}$$

The tensile force that can be resisted by concrete alone in the region where the path changes its direction (in N) is given by

$$V_c=M_c/s \tag{A2}$$

(3) Design of beam I (see Fig. 2c)

Shear Force Sustained by Concrete: For this beam, there are two values of s. For the part of the beam from the left support to the loading point, $s=500$ mm, and for the other part $s=225$ mm.

For $s=500$ mm.

Using Equations A.1 and A.2, $M_C=2871736$ Nmm and $V_c=2871736/500=5743$ N
Applied shear force $V_a=2.86/0.19*0.31*1000$ N$=4666$ N<5743 N
Thus only nominal transverse reinforcement is required.
For $s=225$ mm

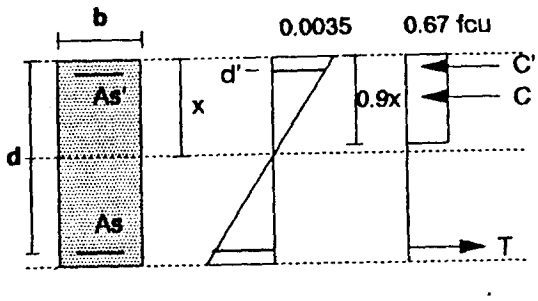

$E = 2 * 10^5$ MPa

$\varepsilon_s = (d-x) * 0.0035 / x$ $f_s = E*\varepsilon_s < f_y$

$\varepsilon_s' = (x-d') * 0.0035 / x$ $f_s' = E*\varepsilon_s' < f_y$

$C = 0.67 * f_{cu} * b * 0.9 * x$

$C' = A_s' * f_s'$

$T = A_s * f_s$

Apply strain compatibility to find x

Then $M_f = A_s * f_s * (d-0.45 * x)+A_s' * f_s'(0.45 * x-d')$

Fig. A1 Flexural capacity of doubly reinforced beams

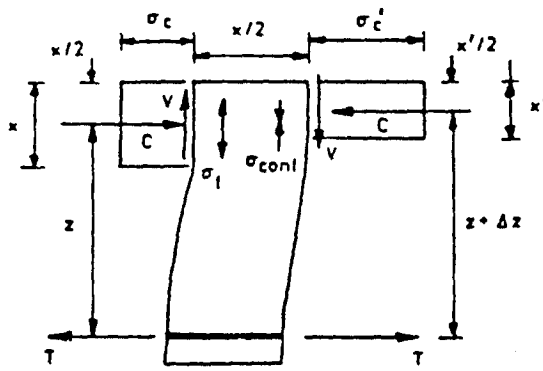

The following steps are to be used:

1. $\Delta z = V*x/(2T)$; $V = V_a - V_c$
2. $x' = 2(d-z-\Delta z) > 0$; if $x' < 0$, increase cross-section
3. Assess nominal triaxial compressive stress σ_c'
   $\sigma_c' = C/(bx')$
4. Assuming 0.8 f_{cyl} describes uniaxial condition (σ_c = 0.8 f_{cyl}), assess confining pressure σ_{conf} required for σ_c to increase to σ_c', from expression
   $\sigma_{conf} = (\sigma_c' - 0.8\ f_{cyl})/5$
5. Assume transverse tensile stress $\sigma_t = -\sigma_{conf}$ (compression positive)
6. Tensile force over length δ will be $T_{sv} = \sigma_t * b * \delta$
7. Amount of transverse reinforcement over length δ to sustain tension T_{sv} will be $A_{sv} = T_{sv} / f_{yv}$

Fig. A2 Assessment of excess tension due to bond failure

Using Equations A.1 and A.2, M_c=1744347 Nmm and V_c=1744347/225=7753 N
Applied shear force V_a=2.86/0.19*0.69*1000 N=10386 N>7753 N
Thus design transverse reinforcement is required.
Transverse Reinforcement:

(i) For excess tension due to change in path direction (see Kotsovos and Lefas 1990, Seraj, Kotsovos and Pavlović 1992a, 1992b, 1993a, 1993b, 1995)
$A_{sv}/S_v=(V_a-V_c)/(f_{yv}*d)$=(10386-7753)/(460*90)=0.0636 mm²/mm, requiring 1.5 mm ϕ two- legged stirrups @ 55 mm c/c.

(ii) For excess tension due to bond failure (see Fig. A2)
$\Delta z=(V_a-V_c)*x/(2T)$=(10386-7753)*15.44/(2*34948)=0.58 mm
$x'=2(d-z-\Delta z)$=2(90-83.05-0.58)=12.74 mm
$\sigma_c'=C/(bx')$=21001/(50*12.74)=32.96 N/mm²
$\sigma_{conf}=(\sigma_c'-0.8\ f_{cyl})/5$=(32.96-28.8)/5=0.83 N/mm²=$-\sigma_t$
Tensile stress resultant over a length of 100 mm=0.83*50*100=4150 N
Required reinforcement per 100 mm length is A_{sv}=4150/460=9.0 mm², which is equivalent to providing 1.5 mm ϕ two-legged stirrups @39 mm c/c.
In Fig. 6b, ϕ1.5-1-45 has been used, averaging the above two requirements (i.e. @55 mm and

@39 mm) for transverse reinforcements, in order to simplify steel placing. The discretized beam II (see Fig. 2c) can be designed in a similar manner.

(4) Design of internal support

At the point of contraflexure, assuming 0.5 N/mm^2 tension will be carried by concrete, A_{sv}/S_v=(10386-0.5*90*50)/(460*90)=0.2 mm^2/mm, requiring ϕ1.5-1-18, as shown in Fig. 3a.

Appendix B

Explanation of the difference between the actual and calculated failure loads of the continuous beams tested

This difference in the experimental and the calculated values is largely due to the use of the elastic moment diagram of Fig. 2b. Since the beam sections above the central support and under the loading points contained the same amount of reinforcement, both in the tension and in the compression side, the moment capacity of all the critical sections was equal. As such, and in view of the above observed discrepancy, it appears that the formation of hinges at all the three peak ordinates of the moment diagram did take place. (The value of the cross-sectional plastic moment was 3.57 kNm.) Furthermore, a closer inspection into the testing set-up of Fig. 3b discloses the fact that the assumed point loading was actually a uniformly distributed load over a width of 40 mm, this being the width of the steel plate through which the loading was transmitted from the jack to the beam; and, since the size of the RC member tested was such that even this small (practically unavoidable) deviation from the theoretically-assumed loading arrangement is important, the magnitude of the peak moment in the plastic moment diagram decreases to 3.46 kNm.

Moreover, if, in the calculation of the flexural capacity of the section, the ultimate failure stress of the longitudinal bars (665 MPa) is used (instead of the average value between yield and ultimate, employed initially), the flexural capacity of the beam section becomes 3.08 kNm, instead of the originally-calculated capacity of 2.86 kNm. This, then, narrows the gap between the above experimental value of 3.46 kNm and the apparent maximum section capacity of 3.08 kNm, i.e. a discrepancy of about 12%.

At loads near failure, triaxial stress conditions exist in the compressive zone of an RC member. Due to the presence of such triaxial stresses, the depth of neutral axis reduces, and consequently the moment capacity of the section increases. Such an increase in the moment capacity of the beam section, at the ultimate limit state, appears to be the only possible explanation that can bridge the gap between the nearest predictions made by the CFP method and the experimental findings.

Appendix C

Validation of the portal frame testing rig

The insignificant amount of recorded out-of-plane displacement due to the applied loading, in comparison to the size of the frames investigated, pointed to the fact that the conditions for applying essentially in-plane vertical and horizontal loadings were fulfilled during testing. Although, during the development of the testing rig, it was planned that the vertical load acting at the mid-section of the beam was to be kept unchanged while laterally loading the frame to failure, it is apparent that the adopted vertical-loading arrangement would be incapable of truly fulfilling the original aim if, at failure, large side sway takes place. This phenomenon can be best explained with reference to Fig. C1. In the figure, C represents the position of the mid-section of the beam at the end of the application of the vertical loading. Since, theoretically, the adopted horizontal loading does not add any moment to the mid-section of the beam element, only pure side sway should take place, without any additional increase in deflection

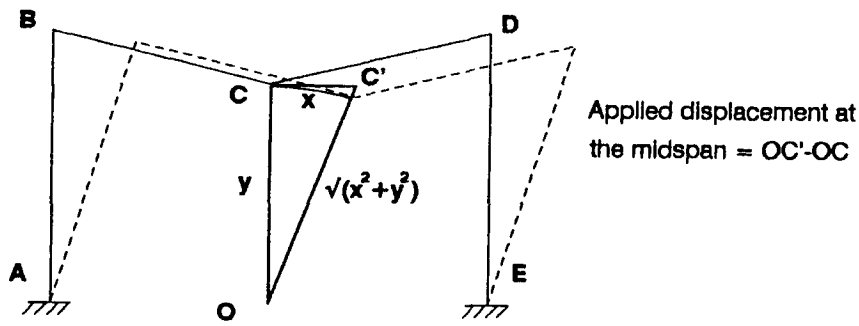

Fig. C1 Pull-down effect due to side sway of portal frame

at the midspan. The point C′ shows such a theoretically expected position of point C at the end of the application of both vertical and horizontal loading. If O is considered as the location of the hinged base of the tension jack, then the length OC (y) represents the height of the beam centre at the end of the vertical-loading application. After a pure side sway of CC′ (x) has taken place, the hypotenuse OC′ of the right-angled triangle OCC′ becomes the new distance of the beam centre from the base of the tension jack. The construction of the rig is such that the length "y" remains unchanged even after side sway has taken place, the vertical load, in the Amsler cabinet, being kept on load maintainer at the end of the application of the vertical load. Thus, at the end of the testing operation, the mid-section of the beam was, in reality, pulled down by an amount approximately equal to the difference of OC′ and OC (shown in Fig. C1, by the curved line). This inadvertently applied vertical displacement subjects the frame to additional vertical loading. The amount of such additional vertical loading is, evidently, less pronounced for small values of side sway; in any case, as the main reinforcements of the frames under investigation were duly instrumented with strain gauges, this additional sway effect could be monitored by estimating the increased moment due to the larger vertical force. Since both frames were tested under identical conditions and were provided with nominal reinforcement capable of sustaining higher stresses than the stresses due to the originally-anticipated design load, the experimental set-up can be considered as acceptable for the present experimental work. It is worth stressing here that the other alternative for applying vertical load to the frame was to apply it by means of a compression jack from a fixed steel girder above the frame. Such an arrangement, however, would be more erroneous, for large side sways, as the point of application of the vertical force would be gradually changed with the progress of the experiment.